Drying Technology
Publication details, including instructions for authors and subscription information:
http://www.informaworld.com/smpp/title~content=t713597247

Experimental Splash Studies of Monodisperse Sprays Impacting Variously Shaped Surfaces

Sam S. Yoon [a]; Ho Y. Kim [a]; Dongjo Lee [a]; Namsoo Kim [a]; Richard A. Jepsen [b]; Scott C. James [c]
[a] Department of Mechanical, Korea University, Sungbukgu, Seoul, Korea [b] Mechanical Environments, Sandia National Labs, Albuquerque, New Mexico [c] Thermal/Fluid Science & Engineering, Sandia National Labs, Livermore, California

Online Publication Date: 01 February 2009

To cite this Article Yoon, Sam S., Kim, Ho Y., Lee, Dongjo, Kim, Namsoo, Jepsen, Richard A. and James, Scott C.(2009)'Experimental Splash Studies of Monodisperse Sprays Impacting Variously Shaped Surfaces',Drying Technology,27:2,258 — 266
To link to this Article: DOI: 10.1080/07373930802606188
URL: http://dx.doi.org/10.1080/07373930802606188

Drying Technology, 27: 258–266, 2009

ISSN: 0737-3937 print/1532-2300 online
DOI: 10.1080/07373930802606188

Taylor & Francis
Taylor & Francis Group

Experimental Splash Studies of Monodisperse Sprays Impacting Variously Shaped Surfaces

Sam S. Yoon,[1] Ho Y. Kim,[1] Dongjo Lee,[1] Namsoo Kim,[1] Richard A. Jepsen,[2] and Scott C. James[3]

[1]*Department of Mechanical, Korea University, Sungbukgu, Seoul, Korea*
[2]*Mechanical Environments, Sandia National Labs, Albuquerque, New Mexico*
[3]*Thermal/Fluid Science & Engineering, Sandia National Labs, Livermore, California*

Despite numerous studies of the drop impact phenomena, studies of the fundamental mechanisms of how the splash corona and subsequent necking yield splashed droplets, not to mention characteristics of these splashed droplets, remain a subject of great interest. Here, we consider a simple question: After impact, what are the characteristics of splashed droplets? Spatial variations in the fraction of splashed liquid, Sauter mean diameter, and drop-size distribution for water and diesel impacting onto variously shaped rods are reported. Liquid drops of nearly uniform size are continuously injected onto a 2-mm-diameter aluminum cylindrical rod at velocities of up to 17 m/s. The impact face of the rod is flat with angles from $\theta = 0$ to 60° or it has a concave, convex, or conical shape. The experimental results indicate that diesel breaks up more easily than water due to its low surface tension. However, due to increased energy loss through viscous dissipation during drop collapse and spreading, dispersion of diesel drops upon and after impact is less energetic than that of water since diesel droplets do not travel as fast or as far as water droplets. During corona formation, stretching and necking of diesel drops before their snap-off are particularly evident due to diesel's high viscosity. Size distribution of splashed diesel droplets is more uniform than that of water near the impact region and water is more uniform further away.

Keywords Diesel spray; Droplet atomization; Splash corona; Viscosity

INTRODUCTION

Drop impact phenomena are encountered in numerous industrial applications such as spray drying,[1–6] pharmaceutical coating,[7–9] inkjet printing, painting, spray cooling, fire suppression,[10,11] and fuel injection systems of internal combustion (IC) engines.[12] It is also relevant to spray-drying applications where powders are produced from suspensions and solutions that are atomized using a various types of atomizers. In these applications, drop-impact phenomena are relevant to minimizing deposits on spray-dryer walls and also to producing powders by spraying monodisperse drops onto various substrates. Drop splashing is also important to IC engine applications because optimization of fuel injection systems for IC engines increases fuel efficiency and controls emissions. When fuel drops continuously impact onto a heated wall inside a combustor, the resulting liquid film results in fuel-rich combustion. This combustion scenario leads to both excessive fuel consumption and substantial emission increases. A desire to reduce emissions has prompted automobile industries to further explore the mechanisms of spray impact inside an engine.[13–24] This fundamental study is also expected to shed light on the common problem in industrial spray dryers that is caused by the impact of droplets on the interior wall of the spray chamber.

In reality, almost all fuel injection systems generate a polydisperse spray with a wide range of drop sizes. To simplify the analysis of spray impact, a monodisperse spray is often considered.[25] Nevertheless, the impact physics of monodisperse spray are often just as complex as those of polydisperse sprays. In fact, even a single drop impact study is far from complete,[26] even though there are significant experimental and numerical studies available to the impact of this type.[27–33] Not surprisingly, studies of how the splashed corona and its necking tendrils lead to splashed droplets, not to mention the characteristics of these splashed droplets, remain areas of active research. Questions arise: Is the liquid volume that remains on the impact surface a function of surface tension or/and viscosity? How do changes in impact speed and impact-surface characteristics complicate the analysis and prediction of drop impact phenomena? These questions will be partly addressed by our experimental studies. While the Leidenfrost effect is important for applications in spray dryers[34] and IC engines,[35] this work will not address the

Correspondence: Sam S. Yoon, Department of Mechanical, Korea University, Anamdong, 5-Ga, Sungbukgu, 136-713, Seoul, Korea; E-mail: skyoon@korea.ac.kr

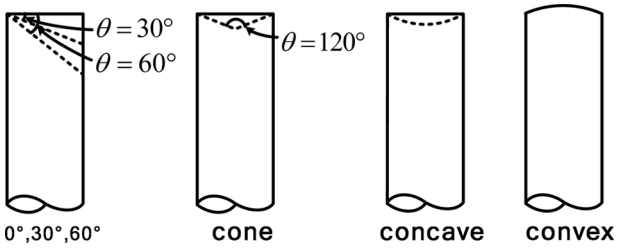

FIG. 1. Shapes of the impact rods.

issue of elevated substrate temperature so that we can focus only on the splash characteristics for water and diesel.

In this work, two major parameters are considered: liquid properties (i.e., surface tension and viscosity) and impact-surface shape. We investigate spatial variations of the splash including the Sauter mean diameter (SMD) and the size distribution for water and diesel drops impacting onto a variety of shapes. Hereinafter, drops refer to the injected fluid (water or diesel) and droplets are those that result from impact. Liquid drops of nearly uniform size (monodisperse) were injected at various speeds onto 2-mm-diameter aluminum cylindrical rods with impact surfaces angled from 0 to 60° or with a horizontal concave, convex, and conical shape, as shown in Figure 1.

EXPERIMENTAL SETUP

A schematic diagram of the experimental apparatus is shown in Figure 2. The liquid was supplied to the atomizer using pressurized nitrogen. A pressure transducer and thermocouples were installed in the liquid supply pipe to measure injection (or operating) pressure and temperature to within 1% error. The volumetric (or mass) flow rate was measured using a gear displacement flowmeter with accuracy also within 1% error.

The monodisperse spray injector, subject to injection gage pressures of 1 to 3 bar, was positioned 10 cm above the top of the impact rod; see Figure 2b. An injection gage pressure of 3.0 bar yielded maximum injection speeds of 16.6 and 17.5 m/s for water and diesel, respectively. To measure droplet characteristics, 10-mm-diameter laser beam transects various x ($0 < x < 8$ cm) and y ($0 < y < 4$ cm) locations at spatial intervals of 10 mm as shown in Figure 2b.

A Malvern particle sizer measures the SMD using Fraunhofer diffraction from a monochromatic light beam. Splashed-droplet diameters, D_s, were fit to a Rosin-Rammler distribution and they typically fell within $30 < D_s < 110\,\mu$m. Based on previous experience,[36] droplet size uncertainty is within $\pm 5\%$ because the detector monitors a statistically reliable average of the light scattering characteristics across several million droplets.

A high-speed CCD camera (500 to 10,000 fps) was used to capture images of the splashing droplets with stroboscopic illumination. All work was conducted at room

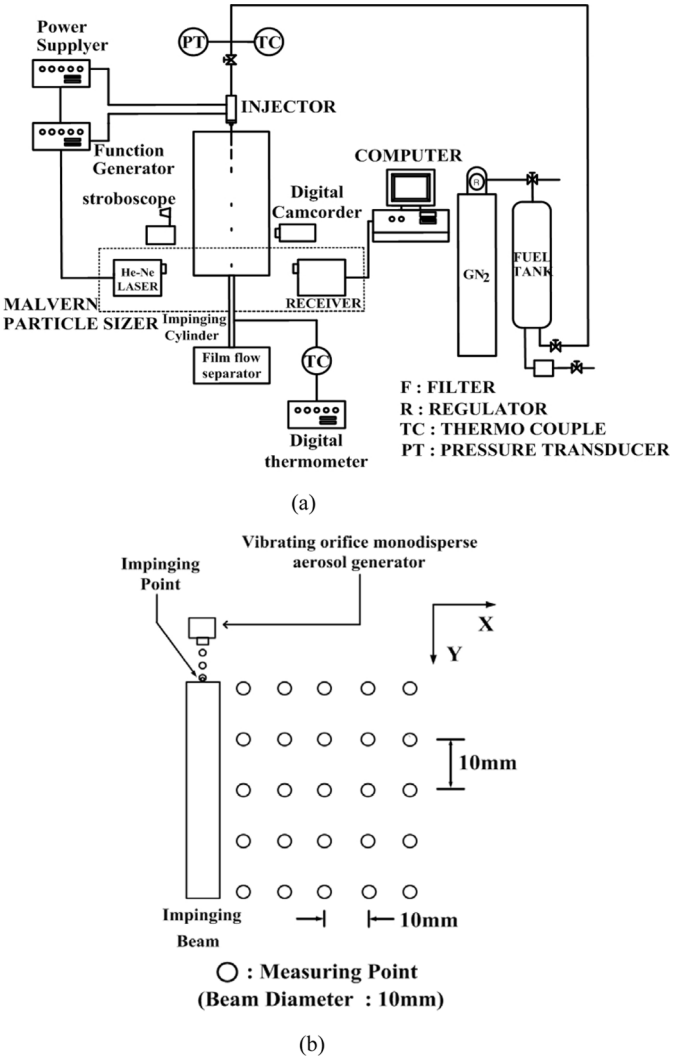

FIG. 2. (a) Schematic of the experimental setup. (b) Droplet measurement points using the Malvern particle sizer.

temperature, although additional lighting could raise local air temperature slightly above 300 K. Nevertheless, thermal evaporation of the splashed droplets was assumed to be negligible; the important parameters governing splashed-droplet characteristics are the impact speed and the shape of the impact surface (not perturbations in local air temperature).

RESULTS AND DISCUSSION

Effect of Surface Tension and Viscosity: Water and Diesel

Figure 3 presents snapshots of water drops impacting onto variously shaped rods when the injected drop size is $D_i = 260 \pm 5\,\mu$m. Under an injection pressure of 1 bar (which generates water drops with velocity $V = 10.4$ m/s), the Weber number is $We = \rho D_i V^2/\sigma = 379$ (where σ and ρ are the surface tension and density of water) and the

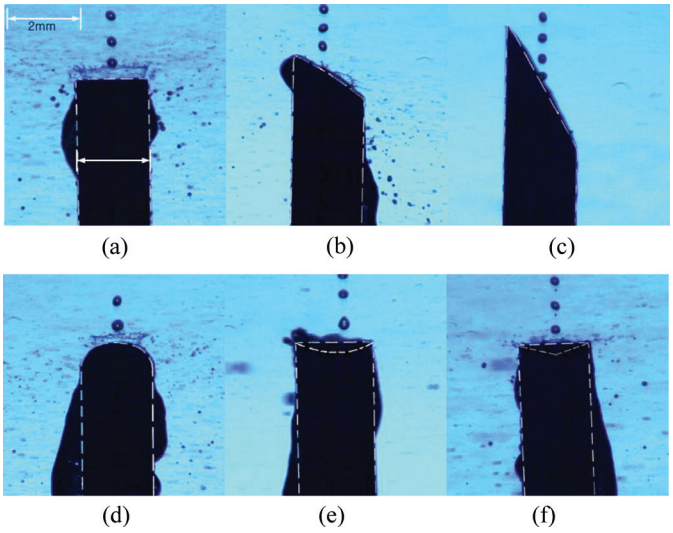

FIG. 3. Snapshots of water drops splashing onto (a) 0°-, (b) 30°-, (c) 60°-, (d) convex-, (e) concave-, and (f) cone-tipped rods. The dashed lines indicate the cross-sectional area of the rods. The black region outside the dashed lines is the dripping liquid.

Reynolds number is $Re = VD_i/\nu = 2{,}370$ (where ν is the water kinematic viscosity). For the flat-tipped rod (or $\theta = 0°$) case, drops clearly produce a corona; see Figure 3a. Increasing the impact angle decreases the magnitude of splashing; see Figures 3b and 3c. When $\theta = 60°$, Figure 3c shows essentially no splashed droplets because the net reaction force approaches zero with increasing impact angle. When the rod tip is convex as in Figure 3d, the splashed corona has a decreased diameter. Post-impact snapshots for concave- and cone-tipped rods are shown in Figures 3e and 3f, respectively, and liquid pools form atop both rods. For the concave-tipped rod, injected drops eject large droplets from the pool. In fact, some of the ejected droplets were larger than the injected drops, as shown in Figure 3e. It is hypothesized that the concave shape lends itself easily to vortex roll-up with consequent ejection of large droplets. The cone-tipped rod, however, does not facilitate sufficient internal vortices, as did in the concave-tipped case.

Figure 4 shows typical snapshots for diesel. Here, as compared to the water case, the Weber number is large ($We = 975$, due to much smaller σ) and the Reynolds number is small ($Re = 352$, due to higher viscosity). For injection pressure of 1 bar (yielding $V = 10.6\,\mathrm{m/s}$ for diesel), incoming drop size is $D_i = 260 \pm 5\,\mu\mathrm{m}$. Note the effect of θ on overall splash phenomena (Figure 4a through 4c); the horizontal force, F_x (and imparted momentum),

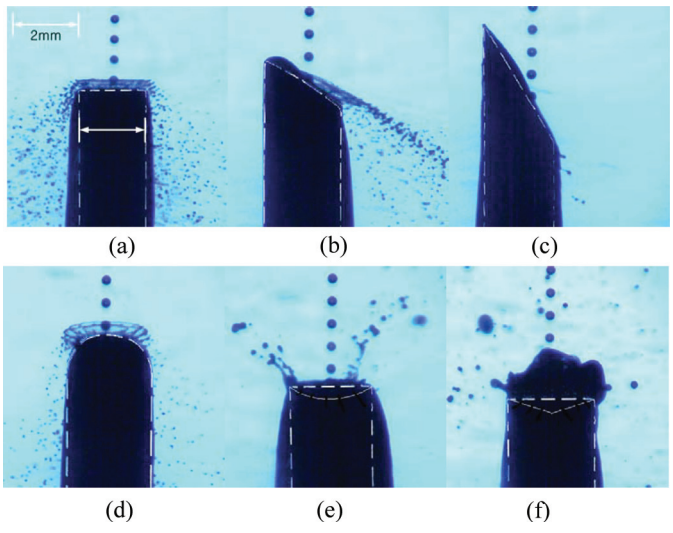

FIG. 4. Snapshots of diesel drops splashing onto (a) 0°-, (b) 30°-, (c) 60°-, (d) convex-, (e) concave-, and (f) cone-tipped rods. The dashed lines indicate the cross-sectional area of the rods. The black region outside the dashed lines is the dripping liquid.

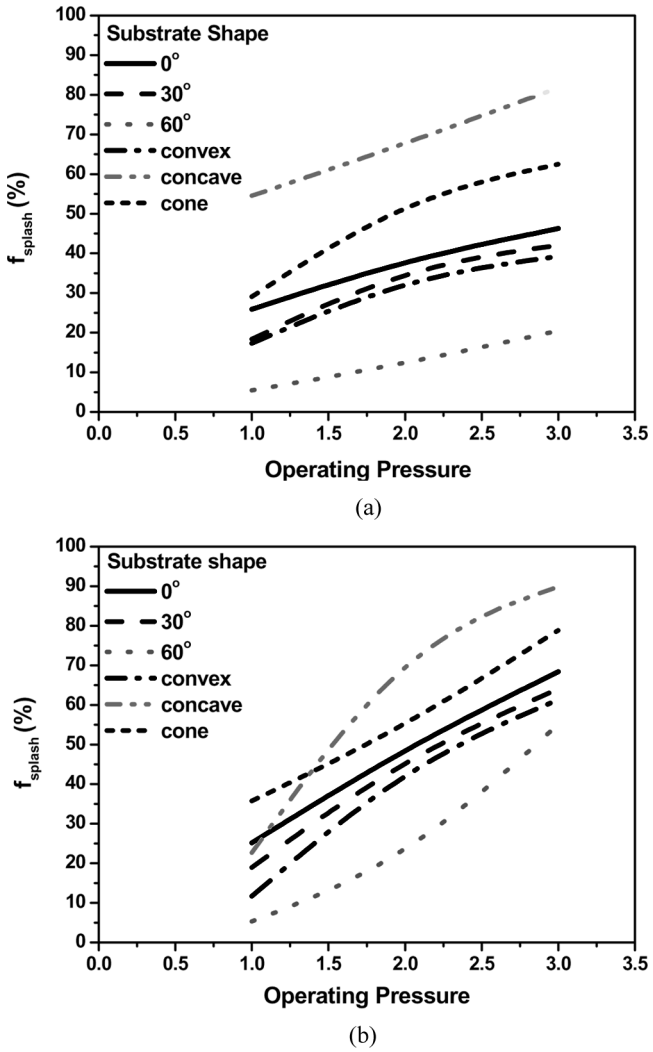

FIG. 5. Splash fraction upon impact onto various rod shapes for (a) water and (b) diesel.

increases up to $\theta = 45^\circ$ since $F_x \propto \sin\theta\cos\theta$. Horizontal ejection of splashed droplets was less evident for water because of its smaller relative *We*; i.e., smaller kinetic energy-to-surface tension ratio. Beyond $\theta = 45^\circ$, horizontally imparted force decreases, resulting in significantly decreased splashing for both water (see Figure 3c) and diesel (see Figure 3c).

Figures 4a and 5b plot the fraction of splashed water and diesel droplets, respectively, as a function of nozzle operating (or injection) pressure for the differently shaped rods. Injected drop diameters remain fairly constant for all pressures. Drops of water and diesel are injected at velocities between 10.4 and 17.5 m/s, yielding Weber numbers ranging from 375 to 876 for water and 915 to 2,370 for diesel. Splash fraction is calculated as

$$f_{splash} = 1 - \frac{\dot{m}_f}{\dot{m}_o}, \tag{1}$$

where $\dot{m}_o$ is the injected total mass flow rate and $\dot{m}_f$ is the mass flow rate collected from drippings off of the bottom of the rod. If all the fluid splashes, then $\dot{m}_f$ would be zero, which yields f_{splash} of unity. Conversely, if no fluid splashes, then all fluid is collected and $\dot{m}_f \to \dot{m}_o$ or $f_{splash} \to 0$.

The splash fraction, f_{splash}, decreases with increasing rod impact angle for both water and diesel; this is because of two competing mechanisms. Horizontal and vertical forces are $F_x \propto \sin\theta\cos\theta$ and $F_y \propto \cos^2\theta$, respectively. As the vertical force decreases, cohesive forces hold more of the impacting fluid on the rod which is ultimately collected at its base.

Of the variously shaped rods, concave tips yield the greatest f_{splash} for both water and diesel. Large splashed droplets appear to be due to injected drops gaining mass due to cohesive forces and vortex roll-up when they impact into the liquid pool. Particularly for diesel, stretching and necking of the corona before complete snap-off (or separation) of the droplets is pronounced; see Figure 4e. Similar behavior was observed occasionally for the cone-tipped rod that also had a liquid pool on it.

Figure 5 reveals notable differences between water and diesel splash fractions. Diesel has slightly smaller f_{splash} than water at low operating pressures and impact speeds, except for the cone-tipped rod. At low impact speeds

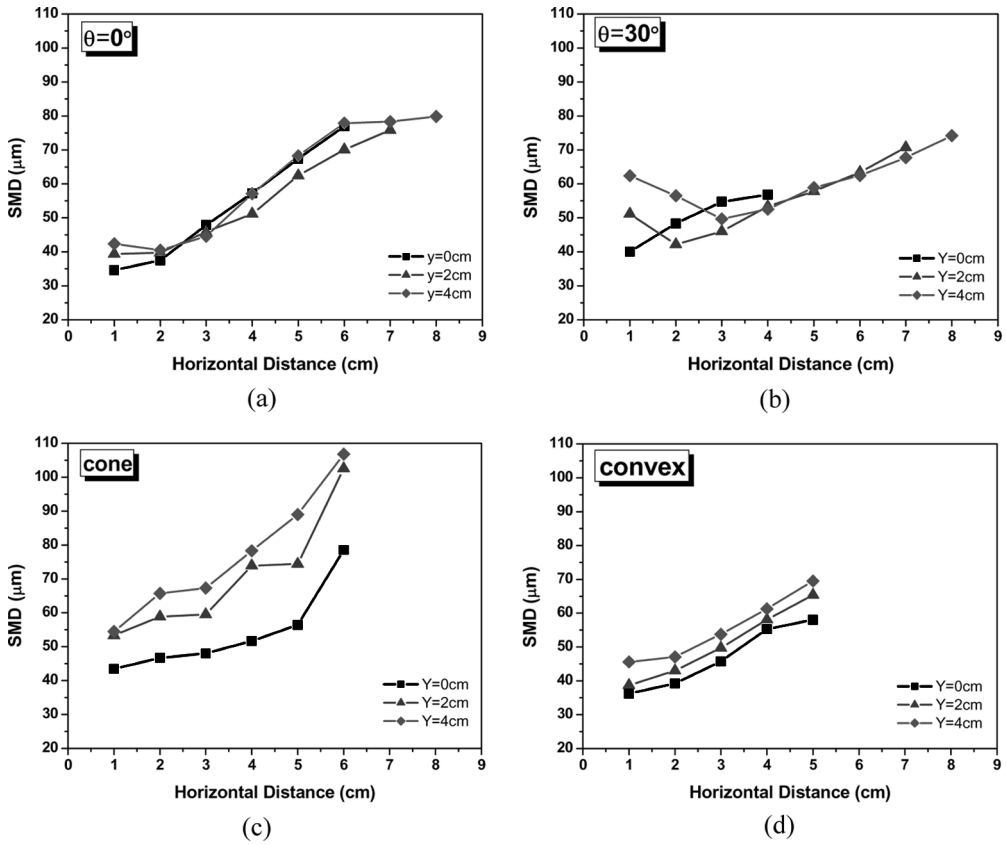

FIG. 6. SMD variations for water droplets at various x and y coordinates for (a) 0°-, (b) 30°-, (c) cone-, and (d) convex-tipped rods.

(~10 m/s), diesel droplets do not splash far with much of the mass simply dripping down the rod and contributing to the non-splashed mass. However, deviations from this trend are observed at higher impact speeds. Diesel's properties (smaller σ) result in a larger *We* than water (for equal impact velocities and drop sizes), implying that it is easier for this fluid to break up into smaller droplets upon impacts at higher velocity (kinetic energy). This effect is more pronounced at higher *We* because $We \propto V^2$. On the other hand, at lower impact speeds, viscous effects (as described by the Reynolds number) dominate; compare coronal stretching and necking between diesel in Figure 4e and water in Figure 3e.

As further evidence, note how diesel in Figure 4d has a larger corona diameter that serves to dissipate the drop's total energy, comprising the kinetic energy, surface tension energy, dissipation energy, and splashing energy. This greater dissipation of the total energy (through corona formation) due to dissipation results in the splashed droplets carrying less momentum. Ultimately, more droplets drip down the rod contributing to greater non-splashed mass as evident in Figure 5b at low injection pressures (i.e., 1 bar).

It is interesting to note that water-drop impacts (at 1 bar; compare Figures 3 and 4) are more dispersive than diesel, which might seem counterintuitive, considering that diesel has a lower surface tension and correspondingly higher Weber number. Diesel's splashing is less dispersive because its viscosity, six times greater than water, and frictionality dissipate more energy as it spreads on the impact surface. Compared to water, diesel loses more energy and momentum during deformation of the impacting drop. Subsequently, much less energy is available for lateral spreading and splashing. Although the surface tension of diesel is about one third that of water, viscous energy dissipation dominates. For these two fluids, it is clear that the larger difference in viscosity (6×) has a more pronounced effect on splashing than the corresponding difference in surface tension (1/3×).

Sauter Mean Diameter of Post-Impact Droplets

Figure 6 (data from Figure 3) shows water SMD increasing with increasing horizontal distance from the impact surface for all rod shapes. Apparently, larger droplets travel further. For $\theta = 0^\circ$- and 30°-tipped rods, it is difficult to infer any discernable effect of vertical

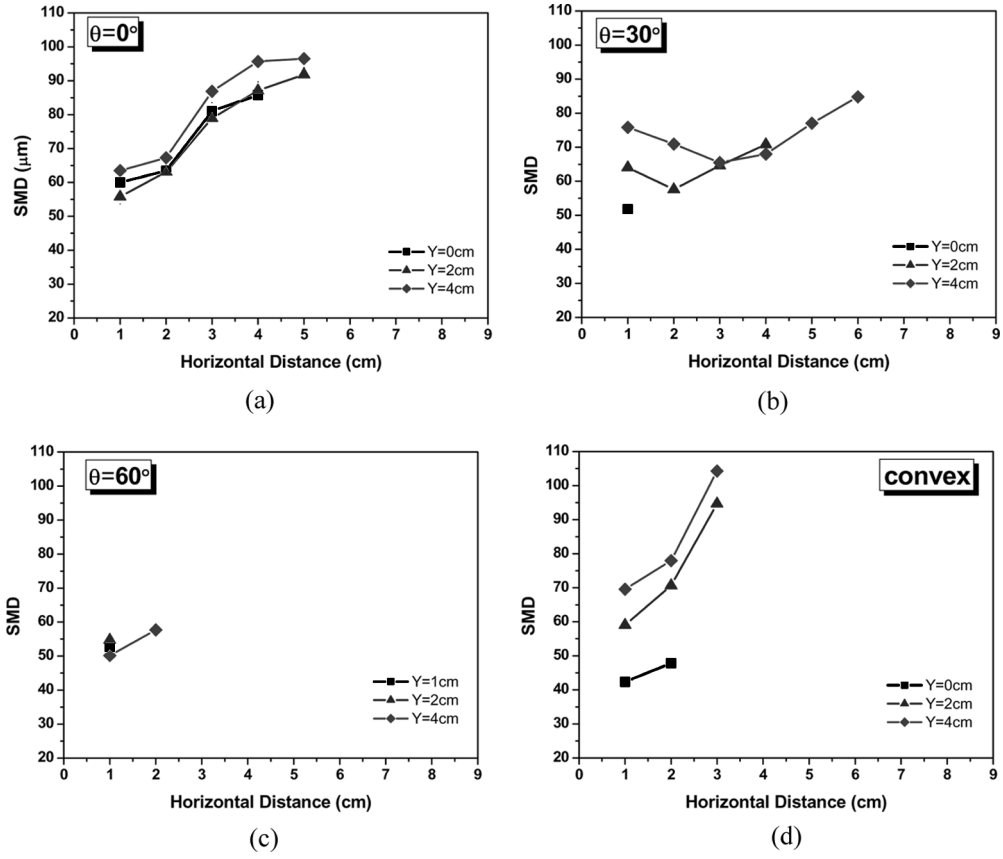

FIG. 7. SMD variations for diesel droplets at various *x* and *y* coordinates for (a) 0°-, (b) 30°-, (c) 60°-, and (d) convex-tipped rods.

locations ($y = 0$, 2, and 4 cm) on SMD. In Figures 6c and 6d, for the cases of convex- and cone-tipped rods, the SMD tends to increase with the increase of vertical direction; i.e., $y = 0$, 2, and 4 cm. Results are not available for the concave- and 60°-tipped rods because splashed droplets rarely intersected the laser beam and it was difficult to measure their representative characteristics.

As the impact angle increases from $\theta = 0^\circ$ to 30° (compare Figures 6a with 6b), larger droplets are observed short horizontal distances from the rod, $1 \leq x \leq 3$. This is because impacts onto the flat rod are more destructive (e.g., $F_y \propto \cos^2 \theta$) and more likely to produce smaller droplets.

Although the horizontal momentum imparted to droplets (i.e., $F_x \propto \sin\theta\cos\theta$) increases as θ changes from 0° to 30°, this effect is not obvious when comparing Figures 6a to 6b. This result is in contrast to that for diesel, which gives higher *We* due to smaller surface tension (see the next section). For the cone-tipped rod in Figure 6c, the pool provides excess liquid, yielding larger droplets. The change in SMD along the vertical direction is more pronounced for the cone-tipped rod. For convex-tipped rods of Figure 6d, ejection energy of splashed droplets is greatly reduced because spreading is radial and downward due to the convex shape of rod (i.e., its shape is ∩). As a result, the horizontal momentum is reduced and droplets do not travel far in the *x*-direction.

Figure 7 is the diesel equivalent to Fig. 6. However, the diesel SMD data for the concave- and cone-tipped rods in Figures 4e and 4f, respectively, could not be measured because the splashed droplets traveled too far in the horizontal direction. SMD data for diesel (Figures 7a, 7b, and 7d) reveal larger droplets than water because diesel's higher viscosity inhibits it from forming small droplets. That is, viscosity dissipates the impact energy, thereby inhibiting formation of many small droplets (consistent with the trend observed in Figure 4). For the convex case in Figure 7d, diesel's SMD is larger than water's, which is shown in Figure 7d. Diesel impacts onto the convex-tipped rod show a greater distinction in SMD along the vertical than does water.

Dispersion Coefficient of Post-Impact Droplets

Figure 8 displays the distribution (or dispersion coefficient) of the Rosin-Rammler distribution for water at various *x* and *y* coordinates, *N*. The larger the *N*, the more uniform the distribution (or smaller width in the

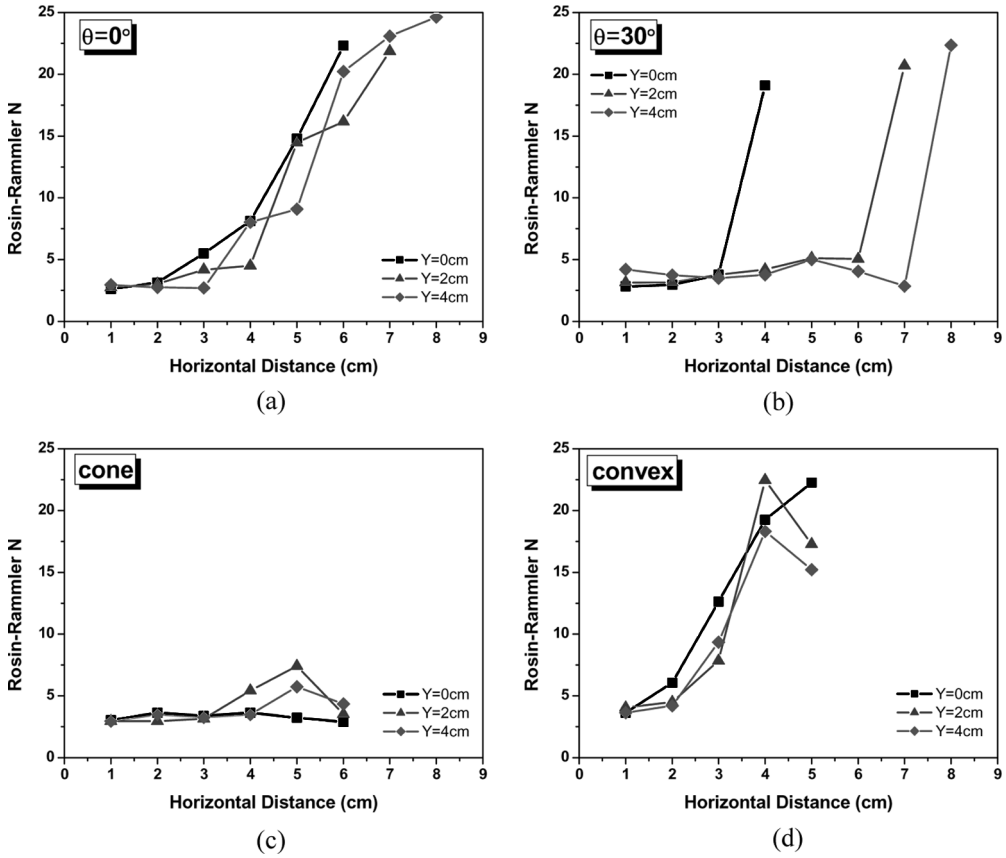

FIG. 8. Variations in dispersion coefficient of the Rosin-Rammler distribution for water droplets at various *x* and *y* coordinates for (a) 0°-, (b) 30°-, (c) cone-, and (d) convex-tipped rods.

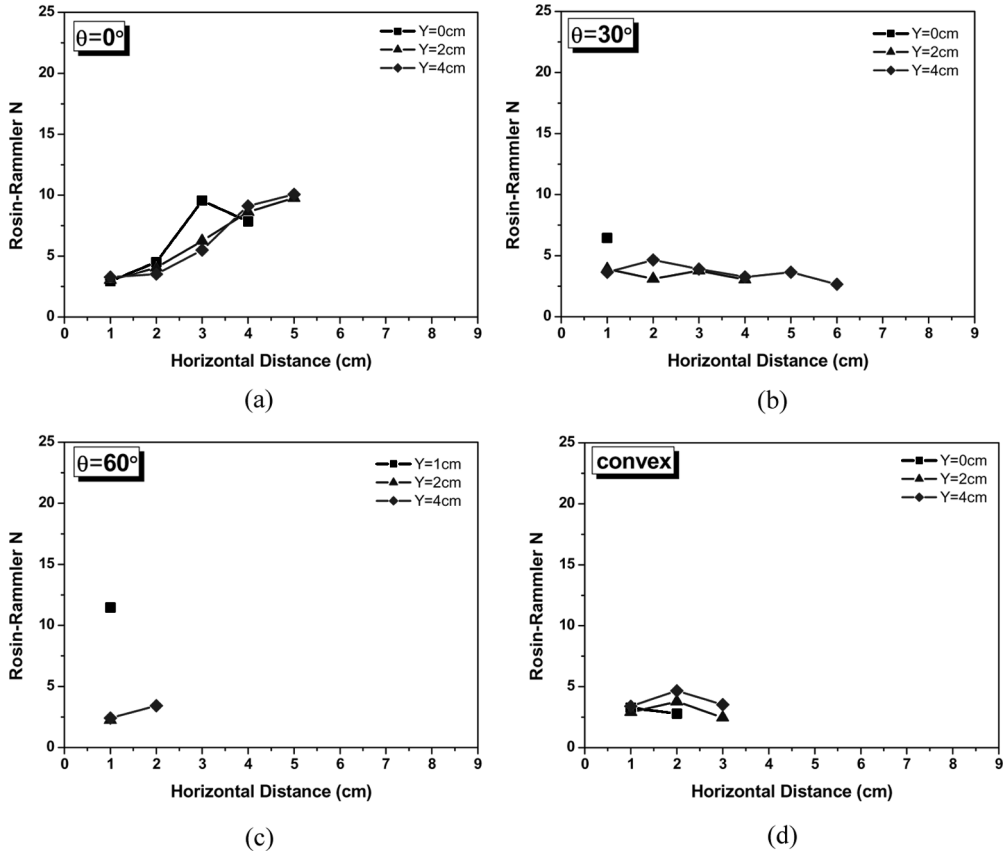

FIG. 9. Variations in dispersion coefficient of the Rosin-Rammler distribution for diesel droplets at various x and y coordinates for (a) 0°-, (b) 30°-, (c) 60°-, and (d) convex-tipped rods.

PDF distribution approaching monodisperse droplets). The Rosin-Rammler probability distribution function, $PDF(D_s) = (ND_s^{N-1}/\overline{D}^N)\exp[-(D_s/\overline{D})^N]$, where D_s is the splashed droplet diameter and $\overline{D}$ is the characteristic or mean droplet size,[37,38] is defined as: $D_{10} = \overline{D}\Gamma(1/N+1)$ or $D_{32} = \lfloor \overline{D}^3\Gamma(3/N+1)\rfloor/\lfloor \overline{D}^2\Gamma(2/N+1)\rfloor$. Here, D_{10} and D_{32} are the arithmetic and Sauter mean diameters, respectively, and $\Gamma(z)$ is the gamma function defined as $\Gamma(z) = \int_0^\infty t^{z-1}e^{-1}dt$.

At the furthest detectable droplet distance in the horizontal direction for $\theta = 0°$-, 30°-, and convex-tipped rods (rightmost points on each curve in Figures 8a, 8b, and 8d), N is fairly large; $N > 15$; the droplets that traveled furthest (largest horizontal distance, x) approach monodispersity. N increases with distance because near the impact, the measurement includes all splashed droplets and further away, only the larger, faster droplets remain, leaving a more narrow distribution of (larger) droplets to measure. For droplets splashing from the cone-tipped rod in Figure 8c, their size distribution is broad ($2 < N < 7$) because the impact is into a fluid pool rather than onto a solid surface. Interestingly, most N values correspond to the Rosin-Rammler distribution function with $N = 3$ at small x distances (near to the rod), which may be related and compared with the predictions of drop-size distribution for film breakup based on percolation theory.[39]

The size distributions of diesel droplets in Figure 9 (the experiment was carried out at the same operating conditions as in Figure 4 of 1 bar) are different from those of water. Specifically, diesel droplets do not travel as far; generally 30 to 40% less than water for each case because of increased energy loss due to viscous dissipation. Shorter splashing distance implies less size size separation and more polydisperse droplets.

CONCLUSION

Monodisperse water and diesel drops ($D_i = 250 \pm 15\,\mu m$) were continuously injected onto 2-mm-diameter aluminum cylindrical rods of various shapes at velocities of up to 17 m/s. The top of the rod was angled from 0 to 60° or its tip was concave, convex, and conical. Spatial variations of the characteristics (such as splashed liquid fraction, SMD, and size distribution) of the splashed droplets were

measured with a Malvern particle sizer. With increasing impact angle, there is less lateral momentum imparted and less splashing is observed. A liquid reservoir was formed for the concave- and cone-tipped rods resulting in drop-onto-pool impacts with behavior substantially differed from that of drop-onto-wall.

At lower impact velocities, the splashed fraction for diesel was similar to that for water and at higher impact speeds diesel splashed fraction was generally greater than that of water. This behavior is explained primarily in light of the significant effects of viscous dissipation; diesel's high viscosity depletes impact energy and precludes the formation of many small drops despite its increased surface tension. Although perhaps counterintuitive, despite diesel's lower surface tension ($\sigma_{water}/\sigma_{diesel} = 2.76$), its drops break up less easily than those of water because of the significant energy dissipation through viscosity ($\nu_{diesel}/\nu_{water} = 6.25$). There is a loss of kinetic energy due to deformation and collapse of the incoming spherical drop into a flat, spreading sheet and subsequent corona formation. It is also notable that measured droplets for both water and diesel are larger and less polydisperse with distance from impact.

ACKNOWLEDGEMENTS

This work was supported by the Korea Science and Engineering Foundation (KOSEF) grant funded by the Korea government (MEST), No. R11-2007-028-03001.

REFERENCES

1. Huang, L.; Kumar, K.; Mujumdar, A.S. Use of computational fluid dynamics to evaluate alternative spray dryer chamber configurations. Drying Technology **2003**, *21*, 385–412.
2. Huang, L.; Mujumdar, A.S. Development of a new innovative conceptual design for horizontal sray dryer via mathematical modeling. Drying Technology **2005**, *23*, 1169–1187.
3. Fletcher, D.F.; Guo, B.; Harvie, D.J.E.; Langrish, T.A.G.; Nijdam, J.J.; Williams, J. What is important in the simulation of spray dryer performance and how do current CFD models perform? Applied Mathematical Modelling **2006**, *30*, 1281–1292.
4. Norton, T.; Sun, D. Computational fluid dynamics (CFD)—An effective and efficient design and analysis tool for the food industry: A review. Trends in Food Science & Technology **2006**, *17*, 600–620.
5. Dalmaz, N.; Ozbelge, H.O.; Eraslan, A.N.; Uludag, Y. Heat and mass transfer mechanisms in drying of a suspension droplet: A new computational model. Drying Technology **2007**, *25*, 391–400.
6. Lagrish, T.A.G. New engineered particles from spray dryers: Research needs in spray drying. Drying Technology **2007**, *25*, 981–993.
7. Jono, K.; Ichikawa, H.; Miyamoto, M.; Fukumori, Y. A review of particulate design for pharmaceutical powders and their production by spouted bed coating. Powder Technology **2000**, *113*, 269–277.
8. Bose, S.; Bogner, R.H. Solventless pharmaceutical coating processes: A review. Pharmaceutical Development and Technology **2007**, *12*, 115–131.
9. Gibbs, B.F.; Kermasha, S.; Alli, I.; Mulligan, C.N. Encapsulation in the food industry: A review. International Journal of Food Sciences and Nutrition **1999**, *50*, 213–224.
10. Yoon, S.S.; Kim H.Y.; Hewson, J.C.; Suo-Anttila, J.M.; Glaze, D.J.; DesJardin, P.E. A modeling investigation of suppressant distribution from a prototype solid-propellant gas-generator suppression system into a simulated aircraft cargo bay. Drying Technology **2007**, *25*, 1021–1033.
11. Yoon, S.S.; DesJardin, P.E.; Presser, C.; Hewson, J.C.; Avedisian, C.T. Numerical modeling and experimental measurements of water spray impact and transport over a cylinder. International Journal of Multiphase Flow **2006**, *32*, 132–157.
12. Panão, M.R.O.; Moreira, A.L.N. Thermo- and fluid dynamics characterization of spray cooling with pulsed sprays. Experimental Thermal and Fluid Science **2005**, *30*, 79–96.
13. Bai, C.; Gosman, A.D. Development of methodology for spray impingement simulation. SAE Paper 1995, 950283.
14. Bai, C.; Gosman, A.D. Mathmatical Modeling of wall films formed by impinging sprays. SAE Paper 1996, 960626.
15. Cossali, G.E.; Marengo, M.; Santini, M. Single-drop empirical models for spray impact on solid walls: A review. Atomization and Sprays **2005**, *15*, 699–736.
16. Kong, S.C. Drop/wall interaction criteria and their applications in diesel spray modeling. Atomization and Sprays **2007**, *17*, 473–499.
17. Naber, J.D.; Enright, B.; Farrell, P. Fuel impingement in a direct injection diesel engine. SAE Paper 1988, 881316.
18. Naber, J.D.; Reitz, R.D. Modeling engine spray/wall impingement. SAE Paper 1988, 880107.
19. Park, K.; Watkins, A.P. Comparison of wall spray impaction models with experimental data on drop velocities and sizes. International Journal of Heat and Fluid Flow **1996**, *17*, 424–439.
20. Stanton, D.; Rutland, C. Modeling fuel film formation and wall interaction in diesel engines. SAE Transactions 1996, 960628.
21. Tropea, C.; Roisman, I.V. Modeling of spray impact on solid surfaces. Atomization and Sprays **2000**, *10*, 387–408.
22. Trujillo, M.F.; Mathews, W.S.; Lee, C.F.; Peters, J.E. Modelling and experiment of impingement and atomization of a liquid spray on a wall. International Journal of Engine Research **2000**, *1*, 87–105.
23. Wang, D.M.; Watkins, A.P. Numerical modeling of diesel spray wall impaction phenomena. International Journal of Heat and Fluid Flow **1993**, *13*, 301–312.
24. Zhou, Q.; Yao, S.C. Group modeling of impacting spray dynamics. International Journal of Heat and Mass Transfer **1992**, *35*, 121–129.
25. Naber, J.D.; Farrell, P.V. Hydrodynamics of droplet impingement on a heated surface. SAE Transactions 1993, 930919.
26. Yarin, A.L. Drop impact dynamics splashing, spreading, receding, bouncing. Annual Review of Fluid Mechanics **2006**, *38*, 159–192.
27. Yarin, A.L.; Weiss, D.A. Impact of drops on solid surfaces: Self-similar capillary waves, and splashing as a new type of kinematic discontinuity. Journal of Fluid Mechanics **1995**, *283*, 141–173.
28. Mundo, C.; Sommerfeld, M.; Tropea, C. Droplet-wall collisions: Experimental studies of the deformation and breakup process. International Journal of Multiphase Flow **1995**, *21*, 151–173.
29. Rozhkov, A.; Prunet-Foch, B.; Vignes-Adler, M. Impact of water drops on small targets. Physics of Fluids **2002**, *14*, 3485–3501.
30. Rozhkov, A.; Prunet-Foch, B.; Vignes-Adler, M. Impact of drops of polymer solutions on small targets. Physics of Fluids **2003**, *15*, 2006–2019.
31. Roisman, I.V.; Horvat, K.; Tropea, C. Spray impact: Rim transverse instability initiating fingering and splash, and description of a secondary spray. Physics of Fluids **2006**, *18*, 102104.
32. Bakshi, S.; Roisman, I.V.; Tropea, C. Investigations on the impact of a drop onto a small spherical target. Physics of Fluids **2007**, *19*, 032102.
33. Okawa, T.; Shiraishi, T.; Mori, T. Effect of impingement angle on the outcome of single water drop impact onto a plane water surface. Experiments in Fluids **2008**, *44*, 331–339.

34. Kudra, T.; Pan, Y.K.; Mujumdar, A.S. Evaporation from single droplets impinging on heated surfaces. Drying Technology **1991**, *9*, 693–707.
35. Choi, K.J.; Yao, S.C. Mechanisms of film boiling heat transfer of normally impacting spray. International Journal of Heat and Mass Transfer **1987**, *30*, 311–318.
36. Park, B.S.; Kim, H.Y.; Yoon, S.S. Transitional instability of a pressure-swirl atomizer due to air-core eruption at low temperature. Atomization and Sprays **2007**, *17*, 551–568.
37. Yoon, S.S.; Heister, S.D. A nonlinear atomization model based on a boundary layer instability mechanism. Physics of Fluids **2004**, *16*, 47–61.
38. Yoon, S.S.; Hewson, J.C.; DesJardin, P.E.; Glaze, D.J.; Black, A.R.; Skaggs, R.R. Numerical modeling and experimental measurements of a high-speed solid-cone water spray for use in fire suppression application. International Journal of Multiphase Flow **2004**, *30*, 1369–1388.
39. Yarin, A.L. *Free Liquid Jets and Films: Hydrodynamics and Rheology*; Longman Scientific & Technical and Wiley & Sons: Harlow, New York, 1993.